Transport mechanisms and effective Schottky barrier height of ZnO/a-Si:H and ZnO/c-Si:H heterojunction solar cells

Asiel N. Corpus-Mendoza, M. M. De Souza, and Frank Hamelmann

Transport mechanisms and effective Schottky barrier height of ZnO/a-Si:H and ZnO/μc-Si:H heterojunction solar cells

Asiel N. Corpus-Mendoza,[1,a)] M. M. De Souza,[1,a)] and Frank Hamelmann[2]

[1]*Electronic and Electrical Engineering Department, University of Sheffield, S1 3JD Sheffield, United Kingdom*
[2]*Department of Technology, University of Applied Sciences Bielefeld Campus, Minden, D-32427 Minden, Germany*

The impact of boron doping on the p-layer of thin film silicon solar cells is assessed by measuring the effective Schottky barrier height of ZnO/a-Si:H and ZnO/μc-Si:H heterojunctions. A deviation from ideal diode characteristics is revealed by an increase of ideality factor with doping concentration. Higher current densities and lower effective Schottky barriers are evaluated for higher doping levels, resulting in increasingly Ohmic behaviour. This is attributed to an enhancement of tunneling through a thinner depletion region, as supported by computer simulations. Extracted barriers are in the range of 0.7–1 eV for the heterojunctions with rectifying behaviour. © 2013 AIP Publishing LLC. [http://dx.doi.org/10.1063/1.4831661]

I. INTRODUCTION

The poor lateral conductance of amorphous silicon in thin film solar cells has been one of the factors driving the use of transparent conductive oxides (TCOs) as contacts covering the entire surface of the semiconductor layers. The smaller thicknesses of the layers in thin film solar cells in comparison to crystalline solar cells also cause a reduced light absorption, which can be alleviated by the light trapping facilitated by the rough structures of the TCO. However, despite the wide optical bandgap and conductivity comparable to that in metals,[1] TCOs such as ZnO produce a Schottky barrier with p-type a-Si:H due to the difference in work function between the two materials. Since an effective p-type TCO for p-layers in solar cells is still under development, methods to lower the Schottky barrier include replacement of the a-Si:H p-type layer with molybdenum oxide (MoO₃), which has a wide bandgap, high work function, and good electrical conductivity.[2] A more widely explored option is the use of interlayers between ZnO and p-type a-Si:H to reduce the barrier height. Some examples of interlayers include n-type μc-Si:H,[3,4] amorphous hydrogenated germanium,[5,6] n-type amorphous tungsten oxide,[7] and metallic nanodots of high work function materials, such as gold, platinum, palladium, or silver.[8] A simpler but still effective approach is addition of a p-type μc-Si:H interlayer between ZnO and a-Si:H.[9,10] The importance of assessing the ZnO/p-type Si Schottky barrier at the interface is essential for the optimization of the solar cell.

In this work, experiments to measure the effective Schottky barrier height of ZnO/a-Si:H and ZnO/μc-Si:H heterojunctions and to identify their transport mechanisms based upon the theory of thermionic emission are performed. Computer simulations considering different transport mechanisms are also used to study the effects of doping on the band diagram of the interface. Finally, both types of structures are tested as window layers for single junction thin film silicon solar cells.

II. EXPERIMENTAL

Three ZnO/a-Si:H and ZnO/μc-Si:H heterojunctions were fabricated. The hydrogen/silane (H₂/SiH₄) ratio was kept constant at 600 for all p-type μc-Si:H layers and at 10 for the p-type a-Si:H layers. The doping concentration of the p-layers was varied by controlling the trimethyl borane (TMB)/silane ratio B(CH₃)₃/SiH₄, which was set to 0.4 for both types of samples. The TMB flow was four times higher for a-Si:H than for μc-Si:H. The standard doping concentrations used for solar cells is referenced to a TMB flow of 100%. The TMB/silane ratio was changed as the TMB flow decreased from 100% to 66% and 33% for both types of p-layers. The area for all samples was 0.008435 cm² with a ZnO layer thickness of 1.8 μm deposited on a thin film of a-Si:H or μc-Si:H layer of thickness 15 nm. Silver was used to contact ZnO and silicon sides on special diode structures fabricated at the same time as the corresponding solar cells, as shown in Fig. 1. Electrical characterization of the samples was conducted by performing dark I–V-T measurements in a cryogenic probe station, in the temperature range 208–318 K. Schottky diode parameters such as the barrier height, ideality factor, and saturation current were calculated using the forward bias region of the I–V curve, which was measured using a Keithley 4200 SCS in the voltage range V = [−1, 2] V with a step of 0.005 V.

III. SCHOTTKY BARRIER DEFINITION

The ideal case of a Schottky barrier at a p-type semiconductor is illustrated in Fig. 2. This barrier height causes rectifying properties at the metal-semiconductor contact, which are ideally defined in Eq. (1) as the difference of the semiconductor valence band and the metal work function, where E_g is the bandgap of the semiconductor

$$\Phi_{bp} = X_S + E_g - \Phi_M. \tag{1}$$

a)Authors to whom correspondence should be addressed. Electronic addresses: dtp10anc@sheffield.ac.uk and m.desouza@sheffield.ac.uk. Tel.: 0044-114 222 58188, Fax: 0114 222 5143.
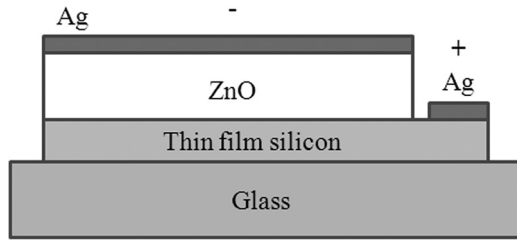
FIG. 1. Schematic diagram of studied structures. Sweep voltage is applied to silver on top of silicon.

The Schottky barrier Φ_{bp} is normally evaluated from I–V measurements, assuming thermionic emission to be the dominant transport mechanism as

$$I = I_0 \exp\left[\frac{q(V - IR_s)}{nkT}\right]\left\{1 - \exp\left[\frac{-q(V - IR_s)}{kT}\right]\right\}, \quad (2)$$

where V is the applied voltage, R_s is the series resistance of the device, and I is the device current, q, k, and T represent the elementary charge, Boltzmann constant, and absolute temperature, respectively. The value n is known as the ideality factor, and for the ideal case of pure thermionic emission, $n = 1$. The term I_0 represents the saturation current and can be related to the height of the Schottky barrier Φ_{bp} as shown in Eq. (3), with A as the area of the device and $A^{**} = 32$ A cm^{-2} K^{-2} as the Richardson constant, for p-type silicon

$$I_0 = AA^{**}T^2 \exp\left(\frac{-q\Phi_{bp}}{kT}\right). \quad (3)$$

The saturation current is evaluated from a plot of ln|I| vs V, where I_0 is found as the intercept of the linear region of the ln|I|-V curve extrapolated to $V = 0$, to then calculate the Schottky barrier height Φ_{bp} from Eq. (3). Also, the ideality factor n can be evaluated from the slope of the linear region as in Eq. (4)

$$n = \frac{q}{kT}\frac{dV}{d\ln(I)}. \quad (4)$$

However, thermionic emission over the barrier as shown in Fig. 2(a) is not the only transport mechanism found in a
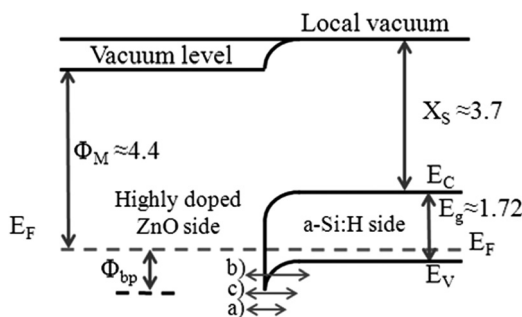

FIG. 2. Metal-semiconductor contact for highly doped ZnO and a-Si:H not drawn to scale. All values are in eV. Horizontal arrows represent the different transport mechanisms present. (a) Thermionic emission over the barrier, (b) field emission or tunneling through the barrier, and (c) thermionic field emission.

metal-semiconductor interface. Field emission can occur if (1) The doping concentration of the semiconductor is high enough to narrow the depletion region, (2) The temperature is sufficiently low to eliminate transport over the barrier, or (3) A large reverse bias is applied. Additionally, an intermediate level known as thermionic field emission is achieved when temperature assisted carriers are able to tunnel through thinner regions of the depletion region.[11,12]

The effect of multiple transport mechanisms is observed as an increase of the ideality factor, and this represents a deviation from pure thermionic emission. Normally, values of n are expected to lie between 1 and 2; however, it is common to find ideality factors even greater than these for amorphous materials,[13,14] attributed mainly to tunneling. As a consequence, the barrier height calculated from Eq. (3) suffers an apparent decrease which seems to contradict Eq. (1). This apparently reduced height (effective Schottky barrier height, Φ_{eff}) results because carriers are able to tunnel through the barrier at lower heights. The value of Φ_{eff} depends on the dominating transport mechanism, unlike the value of Φ_{bp}, which depends on the fundamental properties of the materials.

IV. COMPUTER SIMULATIONS

Besides I–V-T measurements, the effects of doping concentration on the p-type layers of the ZnO/Si heterojunctions were examined by means of Technology Computer Aided Design (TCAD) simulations.[15] Simulations for both types of heterojunctions were conducted and matched in the low voltage range for the forward and reverse bias current obtained from experiments at room temperature (T = 295 K). The low voltage range was chosen to avoid the effects of series resistance of the structure at high voltages. Table I shows a complete list of the parameters used to define ZnO, a-Si:H, and μc-Si:H properties. These values were found to better describe our experiments while keeping the best possible with common values shown in literature.[16–27]

Models used for the simulations include Fermi-Dirac statistics and Shockley-Read-Hall recombination. Amorphous layers were represented by a continuous DOS in the bandgap composed of exponential functions for band tails into the bandgap. Besides the band tails, trap centers distributed as a Gaussian function were inserted in the middle of the gap. These midgap states are donor-like traps charged for electrons but neutral for holes and acceptor-like traps charged for holes but neutral for electrons, which represent the dangling bonds in amorphous materials. Finally, a bandgap narrowing model was included to account for a reduction of bandgap with increasing doping concentration.[28]

V. RESULTS AND DISCUSSION

Fig. 3 shows the experimental |J|-V curves (solid lines) for all ZnO/Si heterojunctions measured at room temperature (T = 295 K), compared with simulations using the values from Table I (open figures). Higher current density levels are observed for μc-Si:H layer in comparison to a-Si:H. This is because the lower bandgap of μc-Si:H (E$_g \approx 1.124$) represents a lower barrier height for holes, as compared to the

TABLE I. List of parameters used or TCAD simulations.[16–27]

Parameter	ZnO	a-Si:H	μc-Si:H
Thickness (μm)	1.8	0.015	0.015
Donor concentration (cm^{-3})	10^{20}		
Acceptor concentration (cm^{-3})		[2×10^{17}, 3×10^{18}]	[10^{17}, 3×10^{19}]
Bandgap (eV)	3.3	1.72	1.124
Electron affinity (eV)	4.35	3.7	4
Effective conduction band density (cm^{-3})	10^{21}	2.5×10^{20}	4.8×10^{19}
Effective valence band density (cm^{-3})	10^{21}	2.5×10^{20}	2.4×10^{19}
Electron mobility (cm^2 V^{-1} s^{-1})	30	10	20
Hole mobility (cm^2 V^{-1} s^{-1})	3	1	5
Band tail states			
Density of states for acceptors (cm^{-3} eV^{-1})		6×10^{19}	9.6×10^{19}
Density of states for donors (cm^{-3} eV^{-1})		9×10^{19}	4.8×10^{19}
Conduction band tail slope (eV)		0.05	0.031
Valence band tail slope (eV)		0.059	0.031
Electron capture cross section for donors (cm^2)		2.5×10^{-15}	2.5×10^{-15}
Hole capture cross section for donors (cm^2)		2.1×10^{-17}	2.1×10^{-17}
Electron capture cross section for acceptors (cm^2)		2.1×10^{-17}	2.1×10^{-17}
Hole capture cross section for acceptors (cm^2)		2.5×10^{-15}	2.5×10^{-15}
Gaussian states			
Peak density of states for acceptors (eV)		8×10^{17}	10^{16}
Peak density of states for donors (eV)		8×10^{17}	10^{16}
Peak energy for donor-like from E$_V$ (eV)		1.24	0.40
Peak energy for acceptor-like from E$_C$ (eV)		1.24	0.45
Standard deviation for Gaussian states (eV)		0.15	0.15
Electron capture cross section for donor (cm^2)		10^{-14}	10^{-14}
Hole capture cross section for donor (cm^2)		10^{-15}	10^{-15}
Electron capture cross section for acceptor (cm^2)		10^{-15}	10^{-15}
Hole capture cross section for acceptor (cm^2)		10^{-14}	10^{-14}

a-Si:H case (E$_g$ ≈ 1.72). According to Eq. (1) and the simulated parameters, barrier height Φ_{bp} values should be approximately 1 eV and 0.7 eV for ZnO/a-Si:H and ZnO/μc-Si:H heterojunctions, respectively. At low doping concentrations, the reverse current is orders of magnitude lower than in the forward case, and a linear region is clearly observed at low positive voltage range, before series resistance becomes dominant. These observations are proof of the rectifying properties of the heterojunctions. Here, thermionic emission over the barrier is expected to play an important role as a transport mechanism. However, as the TMB flow is increased, the linear region in the forward bias is reduced, complicating the evaluation of diode parameters. Also, reverse current density increases up to the point where it reaches almost the same level as the forward current, producing symmetry around V = 0, pointing to additional mechanisms than thermionic emission. This behavior is reproduced in simulations with increase of doping concentration alone.

It can be seen that some of the simulated curves fit better because no attempt has been made to fit other parameters such as bandgap[21] and density of defects with change of doping concentration.[29] The values of doping concentration obtained by matching to experimental data are N$_A$ = 2 × 10^{17} cm^{-3}, N$_A$ = 9 × 10^{17} cm^{-3}, and N$_A$ = 3 × 10^{18} cm^{-3} for the low, medium, and high doping concentrations of a-Si:H layer and N$_A$ = 1 × 10^{17} cm^{-3}, N$_A$ = 1.5 × 10^{19} cm^{-3}, and N$_A$ = 3 × 10^{19} cm^{-3} for low, medium, and high doping concentrations of the μc-Si:H layer, respectively.

Schottky barrier heights Φ_{bp} extracted from simulated energy band diagrams in Fig. 4 are 0.98 eV, 0.96 eV and 0.92 eV and 0.76 eV, 0.57 eV, and 0.41 eV (Fig. 4(b)) for the low, medium, and high doping concentrations of the a-Si:H and μc-Si:H, respectively. The reason why the band diagram for ZnO/a-Si:H samples does not change with doping as much as for ZnO/μc-Si:H samples can be attributed to the poor
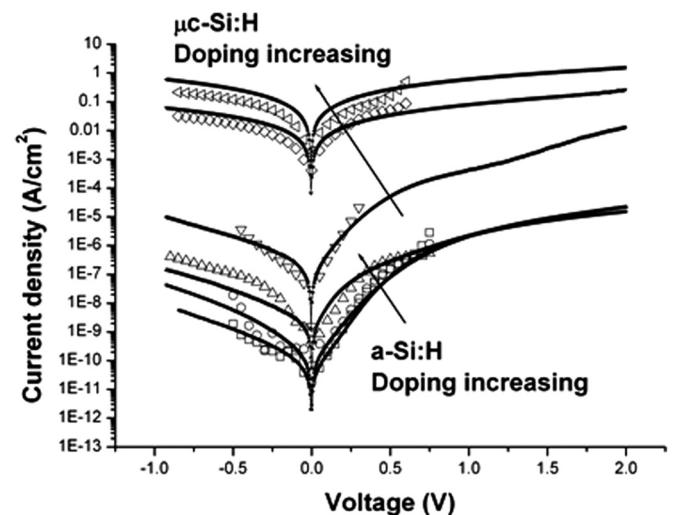

FIG. 3. J-V measurements of all ZnO/μc-Si:H and ZnO/a-Si:H heterojunctions. Current density levels are increased as doping concentration is increased for all samples.
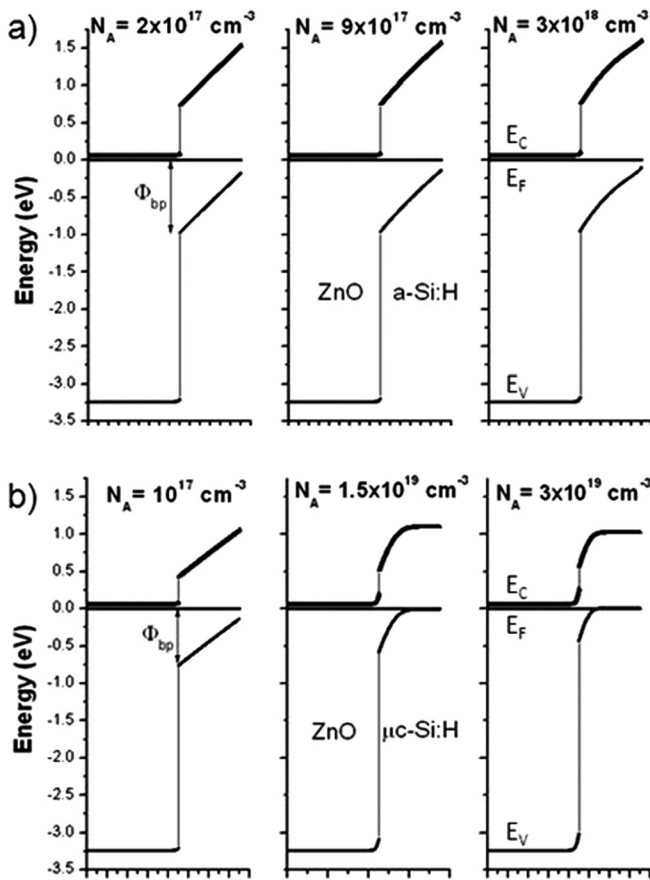
FIG. 4. Energy band diagrams for both types of heterojunctions. Low doping of a-Si:H (15 nm thick) makes its Fermi level to keep almost constant. Since the Fermi level of a-Si:H Fermi is almost at the same position than ZnO work function, a low charge transfer from ZnO to a-Si:H does not produce enough band bending. For ZnO/μc-Si:H samples, a high doping of μc-Si:H reduces the barrier height and makes the depletion region thinner, allowing and increased tunneling transport mechanism.

doping efficiency of a-Si:H. Increasing the doping concentration also has a thinning effect of the depletion region to a point where carriers are able to tunnel through the barrier irrespective of polarity, producing the symmetry around V = 0.

Fig. 5 shows the J-V-T measurements performed for the ZnO/a-Si:H heterojunctions. Steep and clearly defined linear
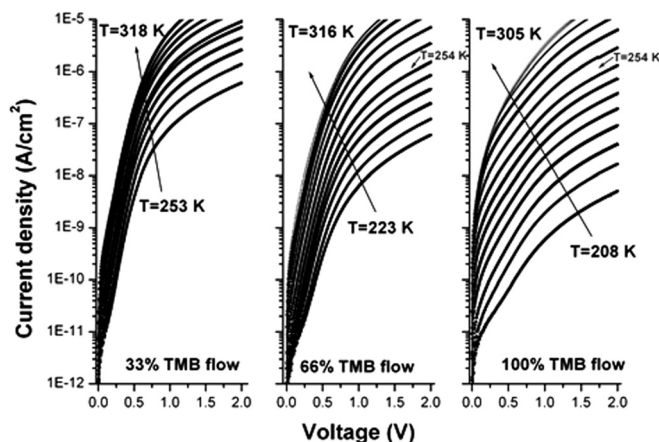

FIG. 5. J-V-T forward bias measurements for ZnO/a-Si:H heterojunctions. Steeper slopes for lower doping concentrations and higher temperatures reveal the influence of thermionic emission transport.
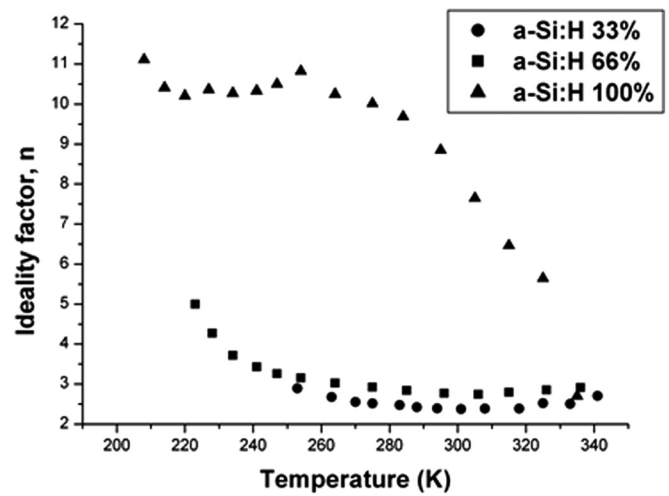

FIG. 6. Influence of thermionic emission transport mechanism is revealed as temperature increases.

regions are observed for the sample with lowest doping concentration at all the temperatures measured. However, as the doping concentration is increased, current density at low voltages rises steeply and causes the slope of the linear region to decrease. This effect combined with the series resistance complicates the identification of the linear region. A reduction of temperature slows the rise of the J-V curve revealing the slope of the curve. Therefore, measurements at lower temperatures are essential for extracting the diode parameters of highly doped samples. These alterations to the curve show that the transport mechanism of the samples changes with doping and also with temperature.

The transport mechanisms can be examined by analyzing the ideality factor described in Eq. (4). Fig. 6 shows that the ideality factor for the three samples decreases towards $n = 1$ as temperature increases. This indicates that thermionic emission becomes more important and more carriers are able to jump over the barrier as the temperature is increased,
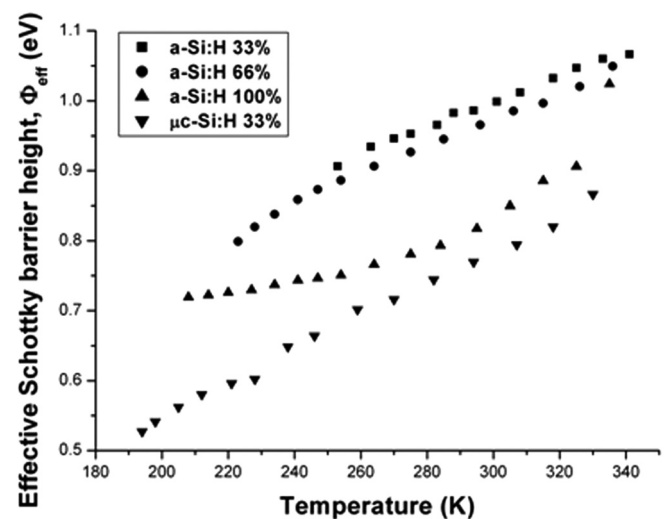

FIG. 7. Effective Schottky barrier height as a function of temperature for the ZnO/a-Si:H structures. The reduction of effective barrier as temperature decreases is attributed to contribution of transport mechanisms such as tunneling.
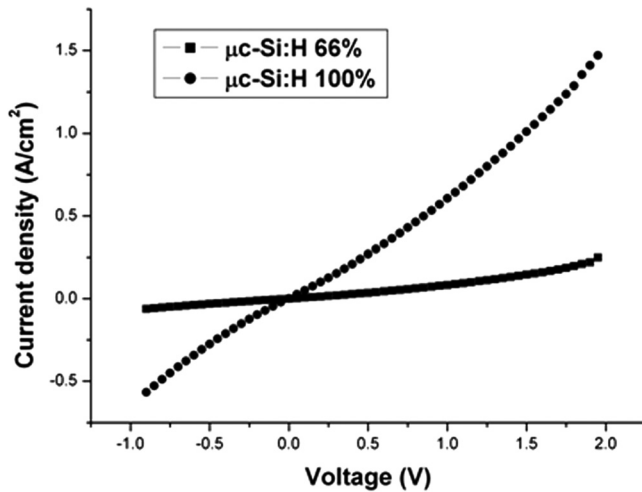
FIG. 8. J-V characteristics for ZnO/μc-Si:H heterojunctions with medium and higher doping concentrations in linear scale. Rectifying characteristics are no longer present for the samples with higher TMB flows. Ohmic characteristics are observed instead.
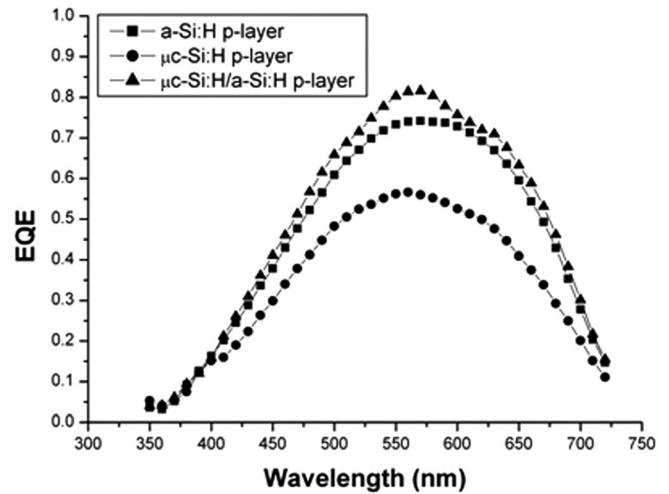

FIG. 9. External quantum efficiency measurements for thin film solar cells with different window layers. Despite the better electrical properties of ZnO/μc-Si:H contact, ZnO/a-Si:H window layer produces better cell performance due to allowing more light to reach the intrinsic region. The best result is obtained for a ZnO/μc-Si:H/a-Si:H window layer.

nevertheless values of $n > 2$ indicate a strong influence of field emission or thermionic field emission. At room temperature, extracted values of $n = 2.39$, $n = 2.77$, and $n = 8.85$ are obtained from the experimental data for the samples with 33%, 66%, and 100% TMB flow, respectively. A strong dependence of Φ_{eff} with temperature is observed from the experimental data in Fig. 7, indicating an increase of Φ_{eff} with temperature. The reason why Φ_{eff} changes with temperature is attributed to the multiple transport mechanisms at the interface.[30,31] At room temperature, the measured values of Φ_{eff} for the ZnO/a-Si:H samples are 0.99 eV, 0.96 eV, and 0.82 eV for the 33%, 66%, and 100% TMB flow, respectively, which agree with the simulated values. Fig. 7 also shows the effective Schottky barrier height for the least doped ZnO/μc-Si:H, since it is the only sample where a linear region could be identified to evaluate the saturation current. The value of Φ_{eff} is found to be 0.77 eV at room temperature.

The increasing symmetry of the ln|J|-V curve around $V = 0$ as the doping is increased is also observed for the ZnO/μc-Si:H heterojunctions, shown in Fig. 3. Linear characteristics can be more easily noted for the two most doped samples when plotted in linear scale as shown in Fig. 8. Since this desired behaviour is more that of an Ohmic than a Schottky contact, the complete loss of the linear region is understood and calculation of ideality factor has no motivation. This does not mean that the μc-Si:H valence band has aligned with the ZnO workfunction. A more appropriate explanation is that the depletion region becomes sufficiently thin to allow for an increased tunneling transport mechanism

regardless of the polarity applied, as shown in Fig. 4. It is reported that a rectifying contact evolves into an Ohmic contact due to tunneling and an apparently reduced barrier height.[12,32]

Finally, the ZnO/Si heterojunctions are tested as window layers for thin film solar cells, with the initial performance shown in Table II. Although the ZnO/μc-Si:H contact has better electrical characteristics than the ZnO/a-Si:H contact, the solar cell using an a-Si:H window layer performs better than the solar cell with a μc-Si:H window. Since the bandgap of a-Si:H is greater than that of μc-Si:H, it allows more light to reach the intrinsic region where the light is absorbed, indicating that there is a trade-off between an Ohmic contact with the TCO and light reaching the absorber layer. This is supported by measurements of external quantum efficiency shown in Fig. 9. However, a positive effect results from a combined μc-Si:H/a-Si:H p-type window layer, since this helps to keep an effectively lower barrier with ZnO without obstructing light from reaching the absorbing layer.

VI. CONCLUSIONS

In summary, the increase of p-layer boron doping reduces of effective Schottky barrier height of ZnO/a-Si:H and ZnO/μc-Si:H heterojunctions, changing their properties from rectifying to Ohmic. An increase of doping also increases the ideality factor evaluated from the J-V curve, revealing an enhanced contribution of tunneling transport mechanism through a thinner depletion region as observed in TCAD simulations. Extracted Schottky barriers are in the range of 0.7–1 eV. The narrow bandgap of μc-Si:H in combination with high doping concentrations produces an Ohmic contact that can be used as a window layer for thin film silicon solar cells however, this reduces the light absorption at the intrinsic region and affects the cell performance. A combination of p-type μc-Si:H/a-Si:H window layer helps to produce an Ohmic contact with the ZnO without compromising the light transmitted to the intrinsic region.

TABLE II. Solar cell parameters using different types of p-type window layers.

Window layer	V_{OC} (mV)	J_{SC} (mA/cm^2)	P_{max} (mW/cm^2)	FF (%)
a-Si:H	852.7	15.15	9.561	74.01
μc-Si:H	828.7	12.65	8.028	76.58
μc-Si:H/a-Si:H	917.1	14.65	10.15	75.55

ACKNOWLEDGMENTS

[1]J. Robertson, R. Gillen, and S. J. Clark, Thin Solid Films **520**, 3714 (2012).

[2]S. Il Park, S. J. Baik, J.-S. Im, L. Fang, J.-W. Jeon, and K. S. Lim, Appl. Phys. Lett. **99**, 063504 (2011).

[3]M. Kubon, E. Boehmer, M. Gastel, F. Siebke, W. Beyer, C. Beneking, and H. Wagner, in *Photovoltaic Energy Conversion, Conference Record of the Twenty Fourth IEEE Photovoltaic Specialists Conference (1994). IEEE First World Conference on Photovoltaic Energy Conversion*, 5–9 Dec 1994.

[4]M. Kubon, E. Boehmer, F. Siebke, B. Rech, C. Beneking, and H. Wagner, Sol. Energy Mater. Sol. Cells **41/42**, 485 (1996).

[5]J. Kim, A. I. Abou-Kandil, A. J. Hong, M. M. Saad, D. K. Sadana, and T.-C. Chen, Appl. Phys. Lett. **99**, 062102 (2011).

[6]G. Ganguly, D. E. Carlson, S. S. Hegedus, D. Ryan, R. G. Gordon, D. Pang, and R. C. Reedy, Appl. Phys. Lett. **85**, 479 (2004).

[7]J.-S. Im, J.-W. Jeon, S. Park, Y. Lee, and K. S. Lim, in *Photovoltaic Specialists Conference (PVSC) (2011) 37th IEEE Photovoltaic Specialists Conference (PVSC)*, Seattle, USA (2011), p. 612.

[8]J. Kim, A. Abou-Kandil, K. Fogel, H. Hovel, and D. K. Sadana, ACS Nano **4**, 7331 (2010).

[9]P.-K. Chang, P.-T. Hsieh, C.-H. Lu, C.-H. Yeh, and M.-P. Houng, Sol. Energy Mater. Sol. Cells **95**, 2659 (2011).

[10]C.-H. Lin, J.-H. Liu, and I. M. Chan, in *Photovoltaic Specialists Conference (PVSC) (2011). 37th IEEE Photovoltaic Specialists Conference (PVSC), Seattle, USA* (2011), p. 3038.

[11]E. H. Rhoderick, IEE Proc., Part I: Solid-State Electron Devices **129**, 1 (1982).

[12]W. B. Jackson, R. J. Nemanich, M. J. Thompson, and B. Wacker, Phys. Rev. B **33**, 6936 (1986).

[13]M. Brötzmann, U. Vetter, and H. Hofsäss, J. Appl. Phys. **106**, 063704 (2009).

[14]A. Madan, W. Czubatyj, and J. Yang, Appl. Phys. Lett. **40**, 234 (1982).

[15]Silvaco, Atlas User's Manual, Device Simulation Software (2009).

[16]M. Vukadinović, F. Smole, and M. Topič, J. Appl. Phys. **96**, 7289 (2004).

[17]N. Hernández-Como and A. Morales-Acevedo, Sol. Energy Mater. Sol. Cells **94**, 62 (2010).

[18]K. Ding, T. Kirchartz, B. E. Pieters, C. Ulbrich, A. M. Ermes, S. Schicho, A. Lambertz, R. Carius, and U. Rau, Sol. Energy Mater. Sol. Cells **95**, 3318 (2011).

[19]A. Fantoni, M. Vieira, and R. Martins, Solid-State Electron. **43**, 1709 (1999).

[20]J. Yuan, H. Shen, L. Lu, T. Wu, and X. He, Optoelectronics and Advanced Materials – Rapid Communications **4**, 1211 (2010).

[21]J. S. C. Prentice, J. Non-Cryst. Solids **262**, 99 (2000).

[22]G. Cannella, F. Principato, M. Foti, S. Di Marco, A. Grasso, and S. Lombardo, J. Appl. Phys. **110**, 024502 (2011).

[23]F. Smole, M. Topič, and J. Furlan, J. Non-Cryst. Solids **194**, 312 (1996).

[24]S. Miyajima, J. Irikawa, A. Yamada, and M. Konagai, J. Appl. Phys. **109**, 054507 (2011).

[25]M. W. M. van Cleef, J. K. Rath, F. a. Rubinelli, C. H. M. van der Werf, R. E. I. Schropp, and W. F. van der Weg, J. Appl. Phys. **82**, 6089 (1997).

[26]M. Nath, P. Roca i Cabarrocas, E. V. Johnson, A. Abramov, and P. Chatterjee, Thin Solid Films **516**, 6974 (2008).

[27]B. E. Pieters, H. Stiebig, M. Zeman, and R. a. C. M. M. van Swaaij, J. Appl. Phys. **105**, 044502 (2009).

[28]T. Krajangsang, I. A. Yunaz, S. Miyajima, and M. Konagai, Curr. Appl. Phys. **10**, S357 (2010).

[29]A. Dussan, R. H. Buitrago, and R. R. Koropecki, Microelectron. J. **39**, 1292 (2008).

[30]D. Donoval, V. Drobny, and M. Luza, Solid-State Electron. **42**, 235 (1998).

[31]D. Donoval, M. Barus, and M. Zdmimal, Solid-State Electron. **34**, 1365 (1991).

[32]K. J. B. M. Nieuwesteeg, M. van der Veen, and T. J. Vink, J. Appl. Phys. **74**, 2572 (1993).